



Article

Experimental and Computational Analysis of Low-Velocity Impact on Carbon-, Glass- and Mixed-Fiber Composite Plates

Ahmed S. AlOmari ^{1,*}, Khaled S. Al-Athel ¹ , Abul Fazal M. Arif ² and Faleh. A. Al-Sulaiman ¹

¹ Mechanical Engineering Department, King Fahd University of Petroleum and Minerals, Dhahran 31261, Saudi Arabia; kathel@kfupm.edu.sa (K.S.A.-A.); falehas@kfupm.edu.sa (F.A.A.-S.)

² McMaster Manufacturing Research Institute, McMaster University, Hamilton, ON L8S 4L8, Canada; afmarif@mcmaster.ca

* Correspondence: alomari@kfshrc.edu.sa; Tel.: +966-11-5577267; Fax: +966-11-5572598

Received: 22 June 2020; Accepted: 10 July 2020; Published: 13 October 2020



Abstract: One of the problems with composites is their weak impact damage resistance and post-impact mechanical properties. Composites are prone to delamination damage when impacted by low-speed projectiles because of the weak through-thickness strength. To combat the problem of delamination damage, composite parts are often over-designed with extra layers. However, this increases the cost, weight, and volume of the composite and, in some cases, may only provide moderate improvements to impact damage resistance. The selection of the optimal parameters for composite plates that give high impact resistance under low-velocity impact loads should consider several factors related to the properties of the materials as well as to how the composite product is manufactured. To obtain the desired impact resistance, it is essential to know the interrelationships between these parameters and the energy absorbed by the composite. Knowing which parameters affect the improvement of the composite impact resistance and which parameters give the most significant effect are the main issues in the composite industry. In this work, the impact response of composite laminates with various stacking sequences and resins was studied with the Instron 9250G drop-tower to determine the energy absorption. Three types of composites were used: carbon-fiber, glass-fiber, and mixed-fiber composite laminates. Also, these composites were characterized by different stacking sequences and resin types. The effect of several composite structural parameters on the absorbed energy of composite plates is studied. A finite element model was then used to find an optimized design with improved impact resistance based on the best attributes found from the experimental testing.

Keywords: composite plate; carbon fiber; glass fiber; impact; finite elements

1. Introduction

Fiber-reinforced composite polymers are used in almost all types of advanced engineering structure. They combine glass or carbon reinforcing fibers with a matrix material such as epoxy, phenolic, or polyester. Composite materials are complex, mainly due to the degree of anisotropy induced by the reinforcing fibers. Thermosetting polymers consist of chain molecules that chemically bond or cross-link with the others when heated together. Composite materials have a high resistance to internal and external corrosion. They are light with a very smooth inside for higher throughputs. Manufacturing a composite structure starts by incorporating a large number of fibers in a thin layer of the matrix to form a ply. The required load in a fiber-reinforced composite structure is obtained by stacking a plurality of layers in a specified order and then grouping them to form a ply. Various layers in a ply can contain fibers in different directions. It is also possible to combine different types of fibers (for example, glass and carbon) to form a hybrid laminate.

A low-velocity impact by foreign objects is a significant concern for composite laminate as this can cause damage to the interior of materials, which significantly reduces the strength of the composite component and may not be easily detected. The complexity of such an impact on composite laminate is due to the different failure modes that occur in composites compared with metals. The selection of optimal parameters for composite plates that give a high resistance to low-velocity impact loads should consider various factors related to the material properties, as well as the manner of manufacturing the composite product. To obtain the desired impact resistance, it is essential to know the correlation between these parameters and the energy absorbed by the composite plate. The development process of this correlation is not an easy task because unknown process parameters are non-linear. Knowing the parameters affecting the impact resistance and the degree to which these parameters affect are the most significant problems of the composite laminate industry.

Drop-weight impact testing is the standard test procedure used to study the impact of resistance and the behavior of composite laminates. Drop-weight testing also tends to be the preferred method when performing low-velocity impact testing. American Society for Testing and Materials (ASTM) Test Method D7136/D7136M [1] is the governing international standard used to study the impact testing on a rectangular plate. This test technique determines the damage resistance of multidirectional polymer matrix composite laminated plates exposed to a drop-weight impact event. The standard test utilizes constant impact energy normalized by specimen thickness. The properties obtained using this test method can guide researchers concerning the anticipated damage resistance of composite structures of similar material, thickness, stacking sequence, and so forth. To compare samples quantitatively, several equations may be used, which can be found in ASTM D7136.

The total amount of energy introduced to a composite specimen and the energy absorbed by the composite specimen through the impact event are essential parameters to assess the impact response of the composite structures. The introduction of new fiber materials is a promising method for strengthening interfacial bonding between the matrix and fibers in hybrid composite laminates. This alteration of the material has been used to enhance the impact resistance of polymer composite materials. A considerable improvement in the impact resistance was achieved by using hybrid composites. The formation of delamination generally relates to matrix cracking. Generally, in any impact situation, matrix cracking occurs first, followed by delamination [2]. Many useful techniques have been successfully devised to improve delamination resistance in the past three decades, namely three-dimensional (3D)-weaving, stitching, braiding, embroidery, Z-pin anchoring, fiber hybridization, toughening the matrix resin, and interleaving with tough polymer, short fibers or micro-scale particles. These methods enhanced the interlaminar properties but at the cost of in-plane mechanical properties [3]. Multiwall carbon nanotube-reinforced carbon-fiber laminates have better energy absorption capacity as compared to neat carbon-reinforced fiber laminate [4]. On the other hand, glass-fiber composites exhibited evident delamination between the plies, matrix transverse cracks within plies, and significant fiber damage at relatively low impact energies [5].

Several low-velocity impact tests considering target size, projectile diameter, and test temperature were carried out by many authors to determine the response of four different combinations of hybrid laminates to low-velocity impact loading using an instrumented impact testing machine [6–9]. Impact resistance is proportional to the thickness of the composite panel, and it was not affected by the geometry of the plate.

New types of fiber materials and different staking were considered [10]. Fiber metal laminate exhibits outstanding impact absorption capacity under various energy levels, where its energy resistance is lower than standard woven fabrics [11]. There is a recent increase in the use of ecofriendly, natural fibers as reinforcement for the fabrication of lightweight with an increasing trend in research publications and activity in the area of basalt fibers. Natural fiber composite has the potential to be widely applied in the alternative to fiberglass composites in sustainable energy impact-absorption structures [12,13]. Deposition of micro- and nano-fillers, such as aluminum powder, colloidal silica, and silicon carbide powder, in glass fiber-reinforced epoxy composites can enhance the impact resistance

and impact energy absorption of the hybrid composite laminates [14,15]. Microencapsulated epoxy and healing agents can be incorporated into a glass fiber-reinforced epoxy matrix to produce a polymer composite capable of self-healing with excellent mechanical strength [16–19].

Sensitivity analysis is one of the approaches that can be used to ascertain the degree of influence of various mechanical and material parameters on the impact performance of the composite laminated plates. Many researchers have tried optimization of the impact performance of the composite plates using the design of experiment (DOE) and artificial neural network (ANN) model with Finite Element Modelling (FEM) techniques. Based on several studies using ANN models to find the optimal laminate combination, the low-velocity impact resistance of fiber-reinforced polymer composite plates depends more significantly on the thickness and the stacking sequence and the effect of the elastic moduli of the fibers. At the same time, the matrix has less effect than the strength of the fiber and matrix materials of the composite [20–23].

Analysis of absorbed energy and velocities during impact testing of composites may not be all that is needed for characterization. For damage mechanism characterization and type of failure identification, post-impact analysis is required to be carried out for the damaged sample [24]. Several techniques were tried and tested and have been proven to provide useful results to characterize the damaged areas in a polymer composite resulting from a low-velocity impact. Visual inspection can be used to analyze the impact tested samples for specific damage types that include dent/depression, cracking/splitting, fiber failure, and delamination. Correlation between detected volumes and absorbed energy using optical measurement is an excellent tool to estimate impact effects [25]. Nowadays, plenty of Non-Destructive Testing (NDT) techniques are investigated for composite inspection [26–31]. Infrared thermography has shown great potential and advantages, which has greater inspection speed, higher resolution and sensitivity, and detectability of inner defect due to heat conduction.

Finite element modeling and simulations are commonly used as well to evaluate the impact resistance of single- and multi-layer fibers [32]. The finite element (FE) model, in conjunction with the material model, is capable of capturing the behavior of composite for multi-layer and stacking configurations under low-velocity impact [33,34].

Others have comprehensively studied the behavior of low-velocity impact on the composites in the literature. However, the current work aims to investigate the impact response of the angle-ply laminated plates using different fibers (carbon and glass). A combination of two types of fibers was also examined. Several types of stacking sequence and resin were considered. Absorbed energy-time curves were presented to understand the behavior of the low impact velocity loading. A flowchart of the entire procedure, experimental and modeling, is given in Figure 1.

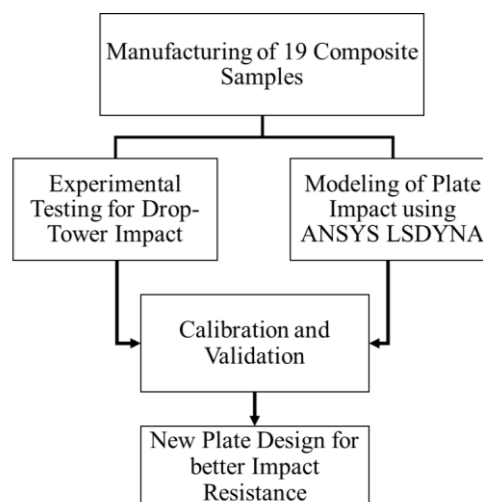


Figure 1. Flowchart for the entire experimental and modeling procedure in this study.

2. Experimental Work

2.1. Materials and Specimen Preparation

The materials in this study consist of woven carbon, glass, and mixed fiber-reinforced laminates, which were manufactured with an asymmetric, quasi-isotropic layup of plies. The glue ratio was 1.1 for the carbon and 0.6 for the glass fiber. Different ply thicknesses and resin types were also considered. Table 1 summarizes the detailed information for the 19-symmetric laminated composite plates that were impact tested. Different stacking sequences characterized these composites. The amount of fiber and resin for each specimen was also considered with different ratios. Note that C stands for carbon-fiber, G stands for glass-fiber, and M stands for mixed-fiber. For matrix material, three types of resin were used, which are epoxy, phenolic (PH), and polyester (PL). The final size of each test specimen is 129 mm by 129 mm.

Table 1. Properties of composite laminates.

Sample No.	Fiber Type (Matrix)	Glue Type (Resin)	Percent Age of Fiber	Percent Age of Epoxy	No. of Layers	Stacking Sequence	Measured Thickness (mm)
C1	Carbon	Epoxy	42.48	57.52	16	[90/−60/−30/0/90/−60/−30/0]s	3.3
C2	Carbon	Epoxy	43.59	56.41	16	[90/0/45/−45/90/0/45/−45]s	3.8
C3	Carbon	Epoxy	45.49	54.51	20	[45/−45/90/0/45/−45/90/0/45/−45]s	4.7
C4	Carbon	Epoxy	45.74	54.26	24	[90/0/45/−45/90/0/45/−45/90/0/45/−45]s	5.5
C4 PH	Carbon	Phenolic	45.74	54.26	24	[90/0/45/−45/90/0/45/−45/90/0/45/−45]s	5.15
C4 PL	Carbon	Polyester	45.74	54.26	24	[90/0/45/−45/90/0/45/−45/90/0/45/−45]s	5.5
C5	Carbon	Epoxy	47.68	52.32	28	[45/−45/90/0/45/−45/90/0/45/−45/90/0/45/−45]s	6.4
C6	Carbon	Epoxy	47.58	52.42	32	[90/0/45/−45/90/0/45/−45/90/0/45/−45/90/0/45/−45]s	7.4
C7	Carbon	Epoxy	45.52	54.48	28	[−45/−60/60/45/−45/−60/60/45/−45/−60/60/45/−45/−60]s	6.6
C8	Carbon	Epoxy	50.00	50.00	32	[60/45/−45/−60/60/45/−45/−60/60/45/−45/−60/60/45/−45/−60]s	7.3
G1	Glass	Epoxy	50.04	49.96	24	[90/0/45/−45/90/0/45/−45/90/0/45/−45]s	4.9
G1 PH	Glass	Phenolic	50.04	49.96	24	[90/0/45/−45/90/0/45/−45/90/0/45/−45]s	5
G1 PL	Glass	Polyester	50.04	49.96	24	[90/0/45/−45/90/0/45/−45/90/0/45/−45]s	4.7
G4	Glass	Epoxy	52.51	47.49	24	[90/−60/−30/0/90/−60/−30/0/90/−60/−30/0]s	5.1
G5	Glass	Epoxy	58.79	41.21	36	[−30/−45/45/30/−30/−45/45/30/−30/−45/45/30/−30/−45/45/30/−30/−45]s	7.1
G6	Glass	Epoxy	66.60	33.40	36	[45/−45/90/0/45/−45/90/0/45/−45/90/0/45/−45/90/0/45/−45/90/0/45/−45]s	7.4
M1	Mixed Carbon-Glass (2 C in the Middle)	Epoxy	62.50	37.50	32	[60/45/−45/−60/60/45/−45/−60/60/45/−45/−60/60/45/−45/−60]s	6.5
M2	Mixed Carbon-Glass (2 C in the Bottom)	Epoxy	62.53	37.47	32	[60/45/−45/−60/60/45/−45/−60/60/45/−45/−60/60/45/−45/−60]s	6.7
M3	Mixed Carbon-Glass (2 C in the Top)	Epoxy	64.51	35.49	32	[60/45/−45/−60/60/45/−45/−60/60/45/−45/−60/60/45/−45/−60]s	6.7

2.2. Low-Velocity Impact Testing

The low-velocity impact tests were performed by an INSTRON Dynatup 9250G (Norwood, MA, USA) drop tower. The impact machine was equipped with a hemispherical impactor head with a diameter of 1 inch. During this test, two types of damages can occur. The first is visible impact damage (CVID), which can easily be seen by the naked eye. The second is barely visible impact damage (BVID), which requires equipment or techniques to capture it. Weights are added to alter the energy of the impact. For all impact tests in this study, the mass of the impactor was 9.2 kg with a constant impact energy level of 20 J, which corresponds to an impact velocity of 2.06 m/s. The impact velocity was measured by a photocell device that is placed in the path of the striker before the impactor strikes the composite plates. The strains measured during impact were loaded into the acquisition software.

The force-time history was measured from the point of initial contact with the plate until the impactor leaves the plate. The energy was calculated from the integration of the force-time signal. The data acquisition system recorded the force-time and energy-time histories. Two rebound arrestors were located on both sides of the composite plate to avoid multiple impacts after the striker rebounds on the plate.

The arrestors were pneumatically actuated, and spring up to separate the impactor from the composite plate after the first impact. Figure 2a shows a schematic picture of the drop weight test. The composite plates to be impacted were positioned under the drop tower using an in-house manufactured specimen fixture where the exposed composite area within the fixture is 110 mm × 110 mm. The composite plates were clamped along all edges. Clamping force was provided by steel plates on the top and bottom edges, as shown in Figure 2b. The clamping force was applied by tightening two bolts at the edge of the fixture.

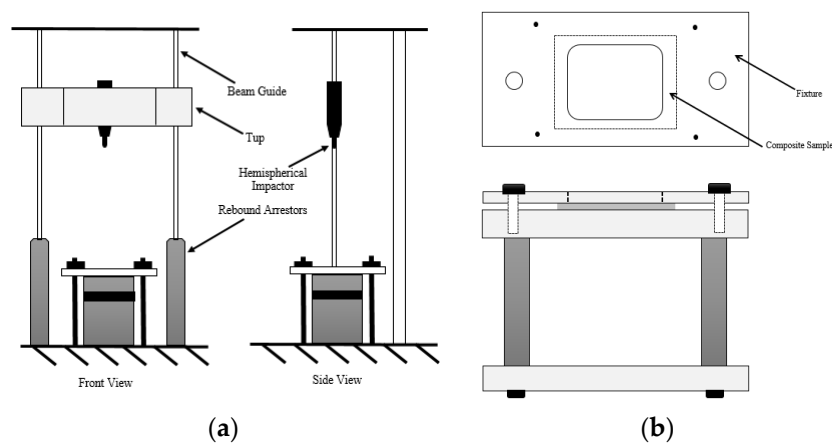


Figure 2. Schematic of (a) drop-weight test, and (b) fixture and sample location.

For the FE model, the plate impact theory is based on the developed theory by Jang et al. [35]. Newton’s second law is used, and the solution for acceleration $a(t)$ is given by:

$$a(t) = g - \frac{P(t)}{M} \tag{1}$$

where g is the gravitational acceleration constant, $P(t)$ is the load as a function of time, and M is the mass of the impactor. At the time when the impact testing starts, $t = 0$ which is known as the initial conditions,

$$v(t) = V \text{ at } t = 0$$

$$x(t) = 0 \text{ at } t = 0$$

where V is the velocity just before impact. The acceleration equation can be integrated to obtain an expression for $v(t)$, and then the velocity equation can also be integrated to obtain a solution for $x(t)$:

$$v(t) = V + \int_0^t g - \frac{P(t)}{M} dt \tag{2}$$

$$x(t) = 0 + \int_0^t v(t) dt \tag{3}$$

It is important to remember that the $x(t)$ equation works as long as the composite plate is not punctured. Once we get $x(t)$, it is easy to solve for the absorbed energy “ E_{absorbed} ” as a function of time.

$$E(t) = \int_0^t P(t)v(t)dt \tag{4}$$

The integration of the energy equation between zero and t , where the impactor is no longer in contact with the composite plate, yields the total energy (E_{total}). The initial velocity v_o is given as a function of gravity and freefall height H as:

$$v_o = \sqrt{2gH} \tag{5}$$

Impactor velocity v and displacement x are calculated by integrating the impact force:

$$v(t) = v_o - \left(\frac{1}{m}\right) \int_0^t P(t)dt \tag{6}$$

$$x(t) = \int_0^t \left(v_o - \left(\frac{1}{m}\right) \int_0^t P(t)dt \right) dt \tag{7}$$

The kinetic energy of the impactor and the absorbed energy are given by:

$$E_{\text{imp}} = \frac{1}{2}mv^2 \tag{8}$$

$$E_{\text{ab}}(t) = \frac{1}{2}mv_o^2 - \frac{1}{2}m\left(v_o - \left(\frac{1}{m}\right) \int_0^t P(t)dt\right)^2 \tag{9}$$

Different results can be obtained from the low-velocity impact test. Typical time versus impact energy and peak loads plots are illustrated in Figure 3 [36]. For the impact energy-time history curve, the highest peak of the curve shows the maximum impact energy, and the end of the curve shows the absorbed energy. The maximum impact is the first impactor kinetic energy, and as the impactor contacts the plate, part of the energy is transferred to the plate. At the end of the impact, not all of the initial kinetic energy is returned to the impactor as part of it is absorbed by processes like plastic deformation and failure of the composite plate. The impact force can be defined by the reaction force between the composite plate and the impactor.

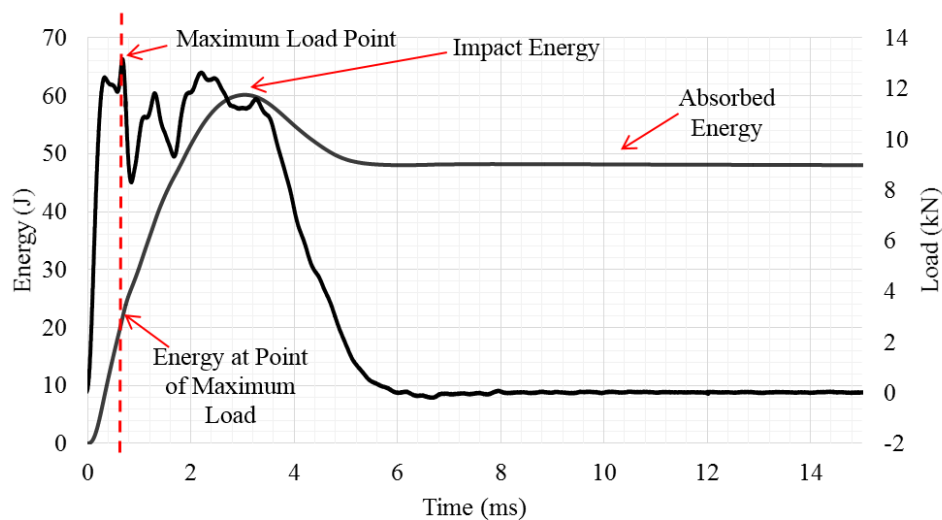


Figure 3. Typical load and energy versus time curve and characteristic points for post-impact analysis.

3. Experimental Results and Discussion

3.1. Low-Velocity Impact Testing

The impact tests were performed using an INSTRON Dynatup 9250G drop tower to determine the amount of impact energy lost in damage during the impact process for each of the defined cases listed in Table 2. Figures 4 and 5 summarize the measured absorbed energies and peak loads, respectively, for all composite samples.

Table 2. Low-velocity impact properties of composite samples.

Sample No.	Peak Load (kN)	Deflection at Peak Load (mm)	Absorbed Energy (J)
C1	4.48	4.97	15.68
C2	4.10	4.69	16.27
C3	5.83	4.67	14.25
C4	7.66	3.42	12.75
C4 PH	5.62	6.63	13.78
C4 PL	8.34	4.16	11.18
C5	9.57	3.03	12.89
C6	11.25	2.68	10.69
C7	9.45	3.18	12.62
C8	11.44	2.73	14.16
G1	7.59	4.90	9.01
G1 PH	5.53	7.47	13.20
G1 PL	7.57	4.97	9.49
G4	7.45	4.76	10.22
G5	10.09	3.24	9.46
G6	9.66	3.19	11.08
M1	9.66	3.19	11.08
M2	8.74	3.53	11.51
M3	8.91	3.47	11.28

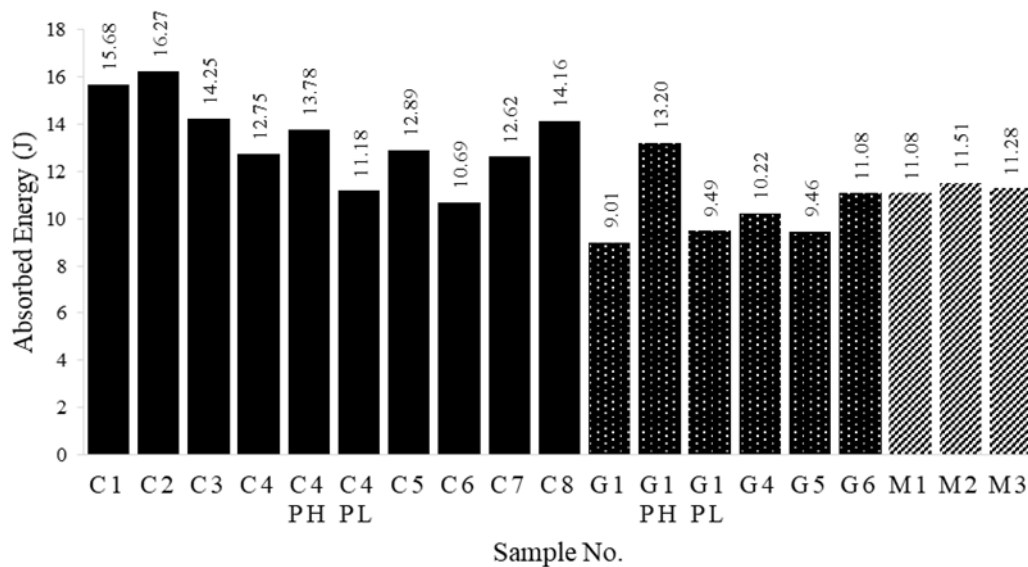


Figure 4. Summary of the measured absorbed energy for all composite plates.

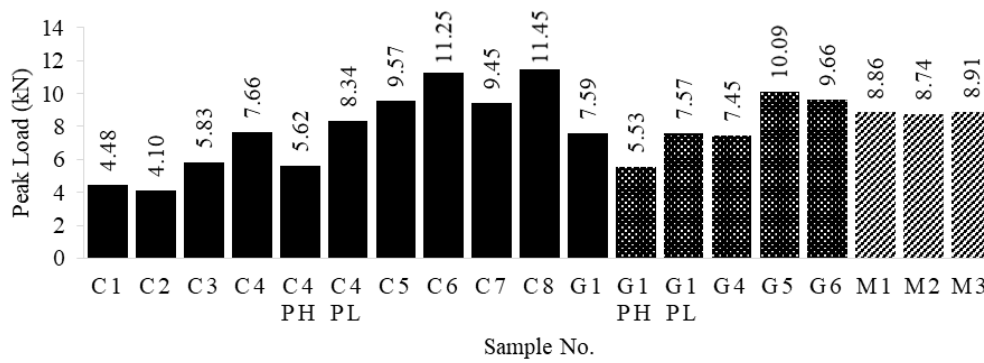


Figure 5. Summary of the measured peak loads for all composite plates.

3.2. Carbon Fiber-Reinforced Polymer (CFRP) Plates

Table 3 and Figure 6 summarize the measured absorbed energies for the tested carbon-fiber plates. The tests show that the impact resistance was affected by the thickness of the plate and the number of plies. It is clear that carbon-fiber composite samples C1, C2, and C3 exhibit the highest absorbed energy. Carbon-fiber plate C2 has the highest measured absorbed energy, then C1, C3, C4 PH, C4, C5, C4 PL, and C7, while C6 has the lowest absorbed energy. The maximum impact force is found to be approximately 11.45 kN for carbon-fiber composite sample C8, while the minimum impact force was measured for carbon-fiber sample C2. The higher impact force is attributed to the energy release due to the composite damage (delamination and matrix cracking). It worth mentioning that there are almost negligible differences in the measured absorbed energies for C5, C4 PL, and C7.

Table 3. Low-velocity impact test conditions and results for carbon-fiber plates.

Sample No.	Absorbed Energy (J)
C1	15.68
C2	16.27
C3	14.25
C4	12.75
C5	12.89
C6	10.69
C7	12.62
C8	10.76

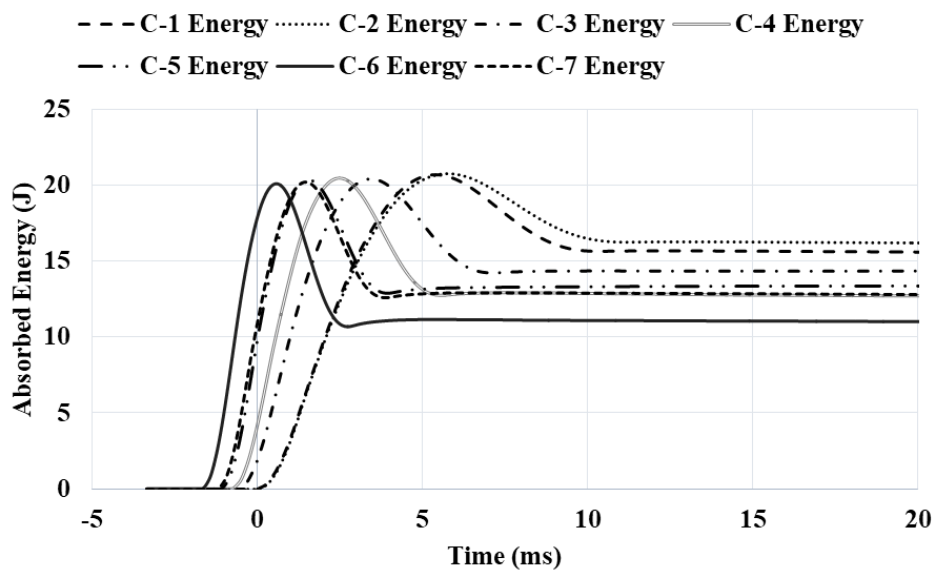


Figure 6. Absorbed energy history of low-velocity impact for different carbon-fiber epoxy plates.

In general, a further increase in the overall thickness of the carbon-fiber plate, either through an increase in layer thickness or by increasing the number of layers, resulting in a decrease in performance. Physically, when the thickness of the composite plate is small, the plate behaves more like a membrane and stretches during impact until all the kinetic energy is transferred to the plate. Then, it pushes back the impactor giving some of the energy back to the impactor, where the rest is dissipated in the form of damage within the plate. The more the thickness of the plate is increased, the stiffer it becomes, and the ability to bend under impact loads is reduced, which increases the bending stress, and hence, the plate suffers more damage. At very high thickness, the plate becomes very strong, which results in deficient amounts of energy absorbed.

Moreover, the energy absorbed in the carbon composites changes with the change in stacking sequence due to the stress redistribution within the laminate. The results show that the minimum amount of energy absorbed is for the case where the laminate configuration is such that the laminate behaves as quasi-isotropic material. The number of layers does not show a linear relation like the stacking sequence. Increasing or decreasing the number of layers by 5%, while keeping the total laminate thickness constant, results in an increased impact energy absorption. Hence, it can be deduced that there must be an optimal number of layers for a fixed thickness, which gives the best impact performance. Thus, there must be an optimal condition for which the amount of absorbed energy and the resulting damage is minimized.

3.3. Glass Fiber-Reinforced Polymer (GFRP) Plates

Table 4 lists the absorbed energies for the glass-fiber plates, while Figure 7 shows the time history of these measured absorbed energies. It was found that G1 PH has the highest measured absorbed energy than G1 PL, G4, G1, G6, while G5 has the lowest absorbed energy. It was expected that the composite plates with glass fiber as the reinforcement material would behave in a similar way to the carbon fiber-based plates. However, it was noticed that the increase in thickness of individual layers increases the absorbed energy. Also, higher energy absorption is seen in [45/−45/90/0]s glass-fiber plates than other stacking sequences, which agrees with the high measured forces of [45/−45/90/0]s glass-fiber composite plate.

Table 4. Measured absorbed energies for glass-fiber plates.

Sample No.	Absorbed Energy (J)
G1	9.00
G4	10.22
G5	9.45
G6	11.08

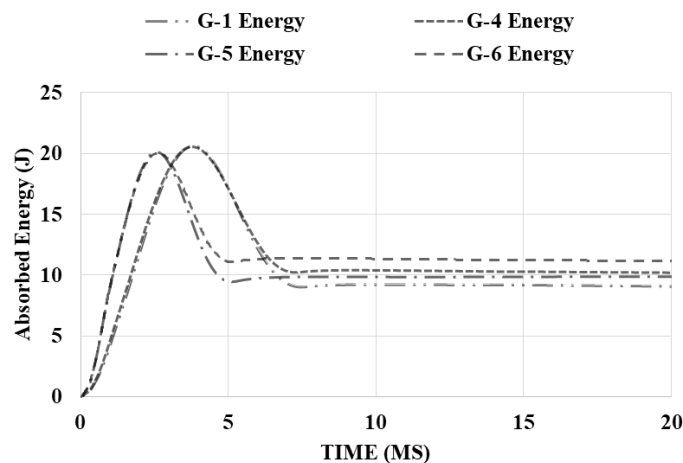


Figure 7. Absorbed energy for different glass-fiber epoxy.

Delamination, crack, or indentation are usually the observed damage forms. If the energy absorbed by the specimen is not too high, the impactor is pushed back, and a rebound occurs. In the case of a rebound, the first drop of force indicates damage to the first material, and the second force drop indicates the failure of the first laminate. Figure 8 shows the extent of the damage for the glass-fiber composite samples (G1, G4, G5, and G6) from the front and back sides. The extent of the damage with the measured absorbed energy can be correlated where the glass-fiber plates with higher absorbed energy show less damage, as in the case of G4.

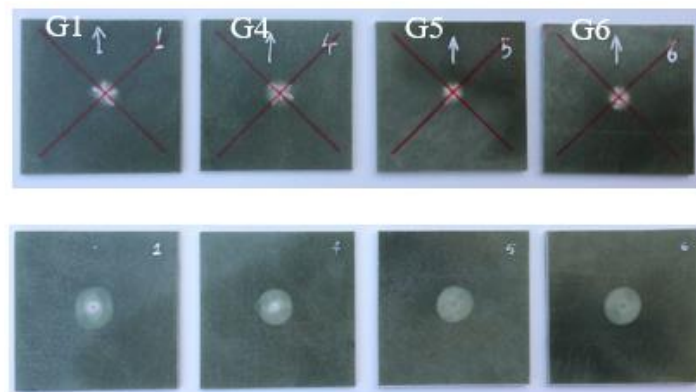


Figure 8. Glass-fiber epoxy plates, (Top: front side, bottom: backside).

3.4. Mixed Fiber-Reinforced Polymer Plates

To understand the relation between the placement of the inclusions and the impact performance, different placements were tried for the carbon layers in the composite plate that mainly consisted of glass fibers. The inclusion of other materials alone cannot guarantee a better performance of the structure, and the placement of the fibers is equally critical. Since the material to be included is based on superior strength and better performance, it should be placed where the damage initiates. The following different combinations were tested with the position of woven carbon lamina as the middle two layers, bottom two layers, and top two-layer. For the aforementioned mixed composite combinations, the glass-fiber composite with two carbon-fiber plies on the bottom has the highest value of the absorbed energy in compression with the same plate with carbon-fiber plies in the middle or at the top. However, the difference is not that pronounced, as can be seen from Table 5 and Figure 9.

Table 5. Low-velocity impact test conditions and results for mixed-fiber plates.

Sample No.	Materials Type	Absorbed Energy (J)
M1	Mixed Carbon–Glass (2 Carbon plies in the middle)	10.82
M2	Mixed Carbon–Glass (2 Carbon plies in the bottom)	11.51
M3	Mixed Carbon–Glass (2 Carbon plies in the top)	11.28

3.5. Effect of Resin Type

A satisfying result was obtained for absorbed energy time given in Table 6 for glass and carbon-fiber plates using different types of resin. It was found that the plate with phenolic resin gives the highest absorbed energy when compared to the epoxy and polyester resins for both glass and carbon composite plates. Moreover, when the force-time history is investigated, the results indicate that composite plates with phenolic resins have the highest resisting force (low peak load), while the composite samples with epoxy and polyester resins have the lowest resisting forces.

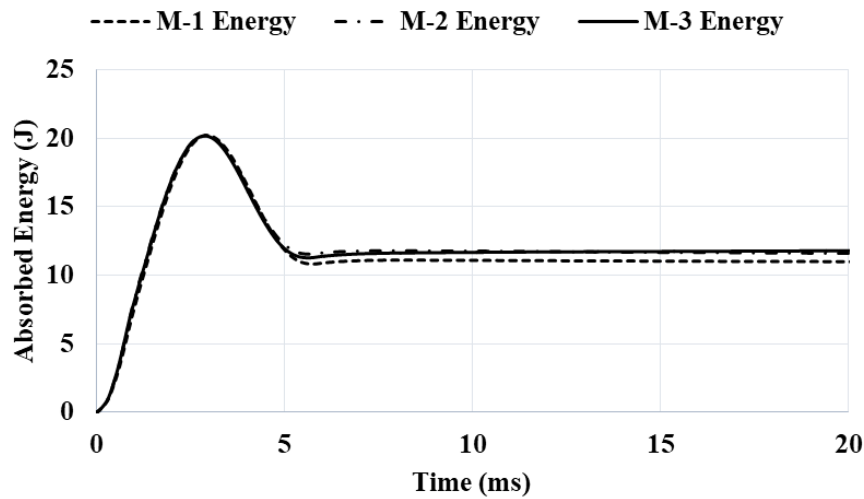


Figure 9. Absorbed energy for different mixed (glass/carbon) fiber epoxy plates.

Table 6. Low-velocity impact test conditions and results for glass- and carbon-fiber plates with different resins.

Sample No.	Fiber Type	Glue Type (Resin)	Peak Load (kN)	Absorbed Energy (J)
G1	Glass	Epoxy	7.59	9.00
G1 PH	Glass	PH	5.53	13.20
G1 PL	Glass	PL	7.57	9.49
C4	Carbon	Epoxy	7.66	12.75
C4 PH	Carbon	PH	5.62	13.78
C4 PL	Carbon	PL	8.34	11.18

Figure 10 shows the surface of the glass-fiber composite plates with different resins (epoxy, polyester, and phenolic) that was tested at the same energy levels. The figure reveals that the plate with phenolic resin shows minimal damage in both the top and bottom sides of the plates. The damage of the glass fiber with epoxy and PL resin samples is observed on both sides of the plate. It is also observed that the damage distribution is much more abundant in the glass-fiber plate with polyester resin than in the glass-fiber epoxy plate.

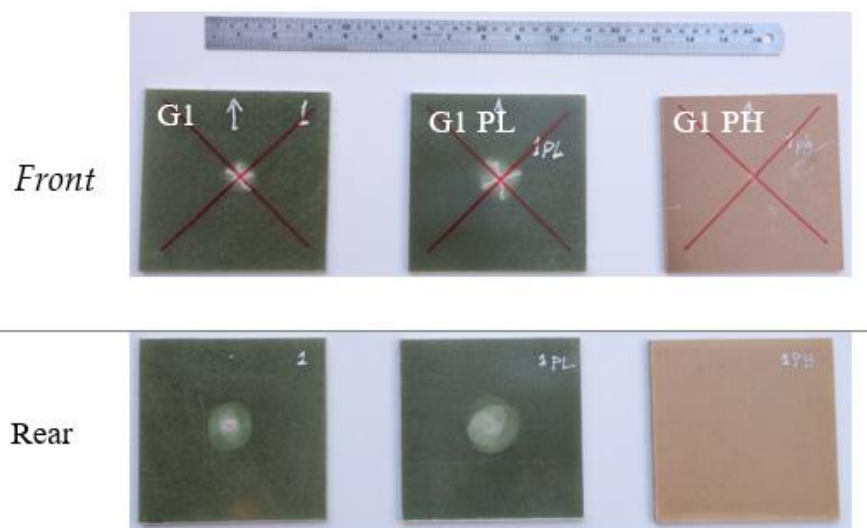


Figure 10. Glass-fiber plates with different resins.

4. Finite Element Modeling

The composite plates were modeled using 3-D shell elements as an area without thickness. The thicknesses and orientations were given as the composite layup data using ANSYS ACP (Canonsburg, PA, USA). The striker was modeled as a 3-D rigid body. Frictionless contact between striker and plate was considered. The amount of damage was calculated as the loss in the kinetic energy of the striker. The FE model is shown in Figure 11.

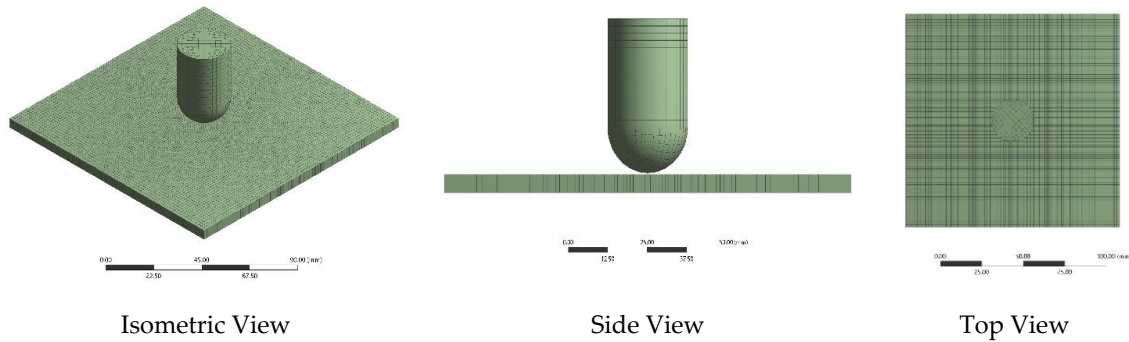


Figure 11. Impact testing modeling using ANSYS LS-DYNA.

In this work, the fixed composite plate was subjected to impact loading represented by the dropped object at a velocity of 2.06 m/s. The impactor (12.7 mm in diameter) was modeled as a rigid hemispherical body. The mechanical properties of the glass and carbon fiber-reinforced composites are listed in Table 7. The initial velocity and mass of the striker were set depending on the energy level considered. The impactor was constrained to movement within 5 degrees of freedom (x and y translations and 3 rotations) and was allowed to move only in the -y-direction. A sufficient density of 7860 kg/m³ was assigned to the rigid impactor.

Table 7. Material properties of epoxy e-glass woven and epoxy carbon woven [37,38].

Property	Epoxy E-Glass Woven	Epoxy CarbonWoven
Density (kg/m ³)	2000	1540
Elastic Properties		
E ₁ (MPa)	50,000	400,000
E ₂ (MPa)	8000	30,000
E ₃ (MPa)	8000	30,000
G ₁₂ (MPa)	5000	6000
G ₂₃ (MPa)	1000	4000
G ₁₃ (MPa)	5000	6000
ν ₁₂	0.3	0.3
ν ₂₃	0.4	0.4
ν ₁₃	0.3	0.3
Ply Strengths		
X _t (MPa)	750	5000
Y _t (MPa)	270	2500
Z _t (MPa)	270	5000
X _c (MPa)	750	5000
Y _c (MPa)	270	2500
Z _c (MPa)	270	5000
S ₁₂ (MPa)	70	400
S ₂₃ (MPa)	30	200
S ₁₃ (MPa)	70	400

The Probabilistic Design System (PDS) module of the commercial finite element software ANSYS was used for the Monte Carlo simulation. A total of 1000 analysis loops are run to obtain the output parameters as a function of the set of random input variables. The 19 plates were manufactured and then tested based on previous work using the Monte Carlo method for random variables to evaluate the effect of variability in the governing parameters for the outcome of the experiment. We selected the von Mises equivalent stress as the outcome of the numerical experiment for the new proposed plates design. To determine the mesh size of elements in finite element modeling, a convergence test was conducted on several cases of the models where Table 8 shows the convergence case for 20 J impact testing. To determine the size of elements in finite element modeling, a convergence test was conducted on several cases of the models where Table 8 shows the case for 20 J impact testing. The analysis showed that, the optimum mesh size was when we selected the axial edge sizing to be 100 divisions with a bias factor of 2.

Table 8. Mesh convergence check for 20 J case.

No of Division for the Axial Edge Sizing	Bias Factor	No. of Elements	Finite Element Modelling (FEM) Absorbed Energy (J)
10	3	100	12.89
25	3	625	11.47
50	3	2500	11.37
75	3	5625	11.13
100	2	10,000	10.68
125	3	12,500	10.68
150	3	15,000	10.68

The simulation was accomplished through a concept known as birth and death of elements in ANSYS. To achieve the “element death” effect, the ANSYS program does not actually remove “killed” elements. Instead, it deactivates them by multiplying their stiffness by a severe reduction factor (ESTIF). This factor is set to 1.0×10^{-6} by default. An element’s strain is also set to zero as soon as that element is killed. In like manner, when elements are “born”, they are not actually added to the model; they are simply reactivated. When an element is reactivated, its stiffness, mass, element loads, etc. return to their full original values.

Contact between the impactor and the whole laminate composite was simulated using the automatic-surface-to-surface penalty-based contact algorithm to accommodate impact initiation and progress. A contact criterion based on 0.01 mm of the normal distance between the contact surfaces was adopted for the simulation. The loads and boundary conditions are shown in Figure 12. The finite element model is generated in ANSYS ACP for angle-ply laminate having different stacking sequences.

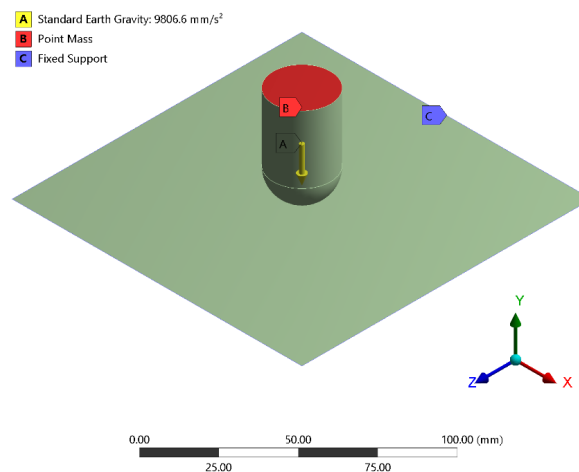


Figure 12. Loading and boundary conditions.

Table 9 lists a comparison of the absorbed energy response, while Figure 13 shows the absorbed energy-time history of the fiberglass plate G4 and Carbon-fiber plate C1 for the case of 20 J obtained by the experiment and by the FE model. The FE results are very close to the experimental values for the final absorbed energy, with an error of less than 9%. This means that the test results validate the FE model. Hereafter, the FE model can be used to perform a parametric analysis; this indicates that the developed FE model can reasonably predict the actual behavior of any composite plate under low-velocity impact loading. The difference in the starting energy time is due to the placement of the impactor close to the plate during modeling to optimize the computational time, whereas in the experiments the impactor falls from a height based on the required energy, which is 20 J in this case. The effect of gravity was considered on the calibration cases for C1 and G1 plates. This is done by including the gravity as an initial condition for the system then by suppressing this feature during analysis. It was found that it is acceptable to ignore gravity as the impact process was performed in a fraction of a second. Including the gravity affects the absorbed energy steady-state line as the bouncing of the impactor decreases with time due to the gravity, and hence the slight inclination in the steady-state line of the absorbed energy.

Table 9. Comparison between the experimental and FE measurement for the absorbed energies.

Sample No.	Experimental Absorbed Energy (J)	FEM Absorbed Energy (J)	ΔE (J)	Percentage %
C1	15.68	16.90	1.28	8.20
G1	10.16	10.68	0.52	5.07

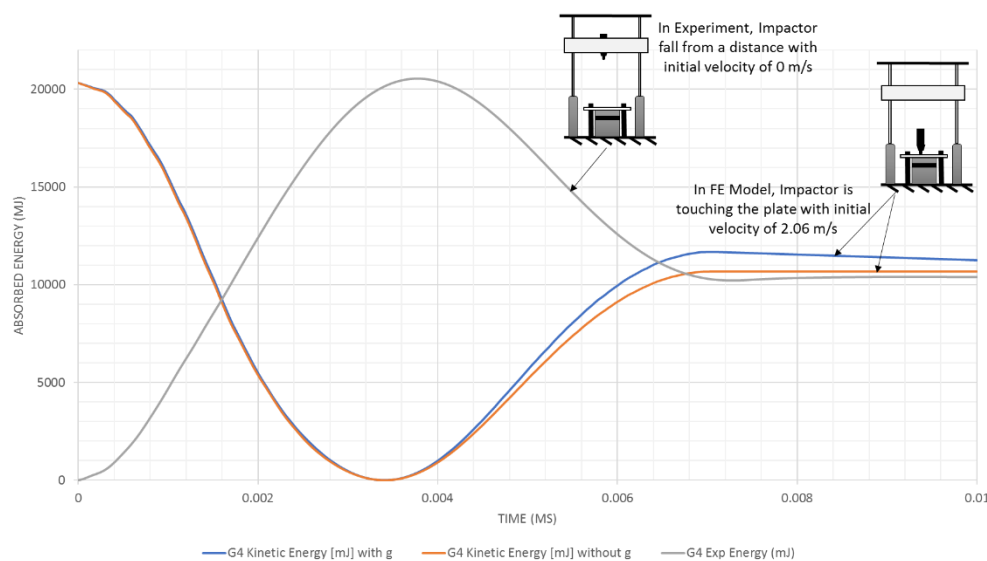


Figure 13. Energy-time curves comparison of the experimental test data and finite element analysis (FEA) data of the G4 fiberglass plate impacted with 20 J.

5. Proposed Design for Composite Plates

It can be concluded from the 19 plate designs and the low-velocity impact tests that the best plate designs with high impact resistance (high absorbed energy), as shown in Table 10, have fewer layers (smaller thickness) with a stacking sequence of [90/0/45/−45]s or [60/45/−45/−60]s. The use of phenolic as a resin gave high impact resistance among all the impacted plates. However, the use of phenolic resin was avoided for the proposed cases as it is costly and not easy to use in manufacturing. Therefore, all cases were modeled with glass-fiber epoxy, as presented in Table 11. The following combinations were adopted for the new designs:

- 16 layers and 24 layers with 3.8 mm and 5 mm plate thickness, respectively.

- Stacking sequence of [90/0/45/−45]s and [60/45/−45/−60]s.

Table 10. Summary of the experimental results for high-performing cases with high absorbed energies.

Sample No.	Peak Load (kN)	Deflection at Peak Load (mm)	Absorbed Energy (J)
C2	4.10	4.69	16.27
C1	4.48	4.97	15.68
C8	11.44	2.73	14.16
G1 PH	5.53	7.47	13.20
M2	8.74	3.53	11.51
G6	9.66	3.19	11.08
G4	7.45	4.76	10.22

Table 11. Proposed new plate designs.

Case No.	No. of Layers	Thickness (mm)	Staking Sequence	Resin/Fiber
Plate-1	16	3.8	90/0/45/−45	Glass Epoxy Woven
Plate-2	16	3.8	60/45/−45/−60	Glass Epoxy Woven
Plate-3	16	5.144	90/0/45/−45	Glass Epoxy Woven
Plate-4	16	5.144	60/45/−45/−60	Glass Epoxy Woven
Plate-5	24	3.8	90/0/45/−45	Glass Epoxy Woven
Plate-6	24	3.8	60/45/−45/−60	Glass Epoxy Woven
Plate-7	24	5.144	90/0/45/−45	Glass Epoxy Woven
Plate-8	24	5.144	60/45/−45/−60	Glass Epoxy Woven

Modeling of the proposed new plate designs reveals that, as shown in Table 12, Plate-7 (with 24 fiberglass plies and a stacking sequence of 90/0/45/−45) has the best design from the impact point of view with predicted absorbed energy of 11.753 J. Figure 14 shows the maximum von Mises (VM) stress distribution for all proposed plate designs, where plates with [60/45/−45/−60]s have lower von Mises stresses when they compared with the plates of [90/0/45/−45]s stacking sequence. In general, [90/0/45/−45]s stacking sequence performed better in impact resistance than [60/45/−45/−60]s for all the simulated cases. Moreover, this design is better than the manufactured fiberglass plates.

Table 12. Summary of the predicted absorbed energy for the new proposed designs.

Case No.	FE Absorbed Energy (J)
Plate-1	9.99
Plate-2	7.47
Plate-3	11.29
Plate-4	9.54
Plate-5	8.87
Plate-6	8.59
Plate-7	11.75
Plate-8	10.44

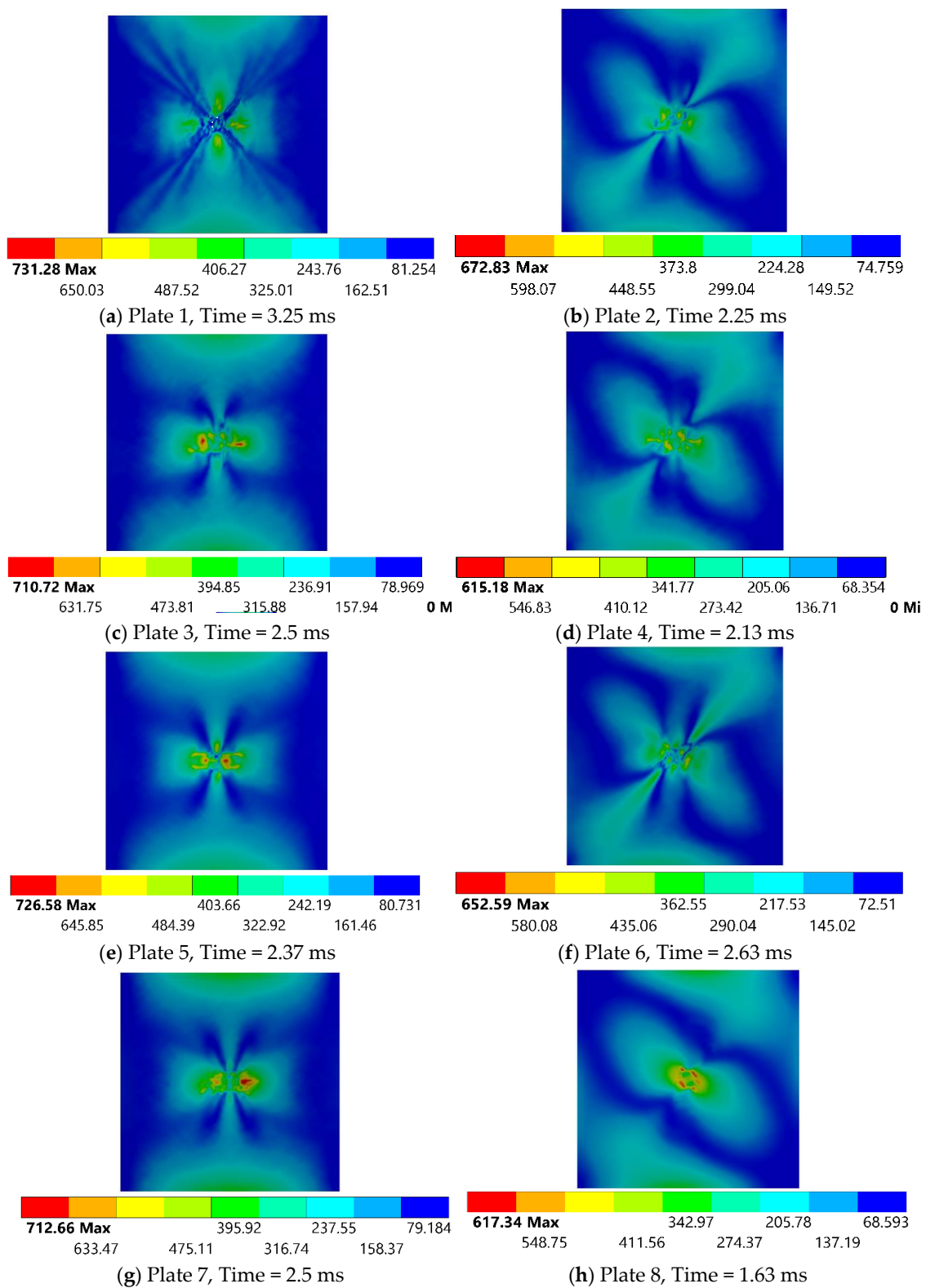


Figure 14. Von Mises stress distribution for all plate designs.

6. Conclusions

In this study, the low-velocity impact behavior of laminated carbon-, glass-, and mixed-fiber plates with different types of resin was investigated experimentally and numerically. The results presented in the current study give an insight into the effects of the considered parameters on the impact-resistance

performance. Several types of stacking sequence at constant impact energy are considered in order to investigate the behavior of composite structures. The main conclusions of the study are:

The amount of energy absorbed (impact performance) varies significantly for the variations in the thickness of a single layer, number of layers, and stacking sequence.

The experimental test data showed an increased energy absorption for the composite plates made with phenolic resin.

The carbon-fiber/epoxy composite plate has better impact resistance compared to the glass-fiber/epoxy composite plate due to the higher measured absorbed energies of the carbon-fiber/epoxy.

Visual inspections showed a large extent of damage was observed on the polyester and epoxy resin plates when they are compared with the same plates made with phenolic resin.

The effect of the carbon-fiber plies location for the mixed plates was not exceptionally pronounced.

The stacking sequence with [90/0/45/−45]s was better than [60/45/−45/−60]s in terms of impact resistance, as concluded from the simulated cases.

The results that were captured from the current work provide a motivation to further examine the samples in the future in order to determine the damage morphology under scanning electron microscopy. Moreover, the results from this study help researchers in designing composite laminated plates with better impact resistance. The results allow for a more methodical approach in selecting the parameters to vary in order to achieve better impact performance of composite laminates against low-velocity impact loadings.

Author Contributions: Conceptualization, A.F.M.A. and A.S.A.; methodology, A.S.A.; software, A.S.A.; validation A.S.A., K.S.A.-A., and A.F.M.A.; formal analysis; writing—original draft preparation, A.S.A.; writing—review and editing, K.S.A.-A.; supervision, A.F.M.A.; project administration, F.A.A.-S.; All authors have read and agreed to the published version of the manuscript.

Funding: This research received no external funding.

Acknowledgments: The authors gratefully acknowledge the support of F.A.A.-S for providing the composite sample plates.

Conflicts of Interest: The authors declare no conflict of interest.

References

1. ASTM D7136/D7136M, Standard Test. *Method for Measuring the Damage Resistance of a Fiber-Reinforced Polymer Matrix Composite to a Drop-Weight Impact Event*; ASTM International: West Kanhohoken, PA, USA, 2005.
2. Khan, S.H.; Sharma, A.; Parameswaran, V. An Impact Induced Damage in Composite Laminates with Intra-layer and Inter-laminate Damage. *Procedia Eng.* **2017**, *173*, 409–416. [[CrossRef](#)]
3. Khan, S.U.; Kim, J.-K. Impact and Delamination Failure of Multiscale Carbon Nanotube-Fiber Reinforced Polymer Composites: A Review. *Int. J. Aeronaut. Space Sci.* **2011**, *12*, 115–133. [[CrossRef](#)]
4. Rawat, P.; Singh, K.K. Damage Tolerance of Carbon Fiber Woven Composite Doped with MWCNTs under Low-velocity Impact. *Procedia Eng.* **2017**, *173*. [[CrossRef](#)]
5. Selver, E.; Potluri, P.; Hogg, P.; Soutis, C.; Soutis, C. Impact damage tolerance of thermoset composites reinforced with hybrid commingled yarns. *Compos. Part B Eng.* **2016**, *91*, 522–538. [[CrossRef](#)]
6. Hosur, M.; Adbullah, M.; Jeelani, S. Studies on the low-velocity impact response of woven hybrid composites. *Compos. Struct.* **2005**, *67*, 253–262. [[CrossRef](#)]
7. Yang, F.; Cantwell, W. Impact damage initiation in composite materials. *Compos. Sci. Technol.* **2010**, *70*, 336–342. [[CrossRef](#)]
8. KERŠYS, A.; Keršien, N.; Žiliukas, A. Experimental Research of the Impact Response of E-Glass/Epoxy and Carbon/Epoxy Composite Systems. *Mater. Sci.* **2010**, *16*, 324–329.
9. Rilo, N.F.; Ferreira, L.M.S. Experimental study of low-velocity impacts on glass-epoxy laminated composite plates. *Int. J. Mech. Mater. Des.* **2008**, *4*, 291–300. [[CrossRef](#)]
10. Asaee, Z.; Shadlou, S.; Taheri, F. Low-velocity impact response of fiberglass/magnesium FMLs with a new 3D fiberglass fabric. *Compos. Struct.* **2015**, *122*, 155–165. [[CrossRef](#)]

11. Asaee, Z.; Taheri, F. Experimental and numerical investigation into the influence of stacking sequence on the low-velocity impact response of new 3D FMLs. *Compos. Struct.* **2016**, *140*, 136–146. [[CrossRef](#)]
12. Boria, S.; Santulli, C.; Sarasini, F.; Tirillò, J.; Caruso, P.; Infantino, M. Potential of wool felts in combination with glass fibers: Mechanical and low-velocity impact assessment. *Compos. Part B Eng.* **2017**, *118*, 158–168. [[CrossRef](#)]
13. Caprino, G.; Carrino, L.; Durante, M.; Langella, A.; Lopresto, V. Low impact behavior of hemp fiber reinforced epoxy composites. *Compos. Struct.* **2015**, *133*, 892–901. [[CrossRef](#)]
14. Rafiq, A.; Merah, N.; Boukhili, R.; Al-Qadhi, M. Impact resistance of hybrid glass fiber reinforced epoxy/nanoclay composite. *Polym. Test.* **2017**, *57*, 1–11. [[CrossRef](#)]
15. Haro, E.; Odeshi, A.; Szpunar, J.A. The energy absorption behavior of hybrid composite laminates containing nano-fillers under ballistic impact. *Int. J. Impact Eng.* **2016**, *96*, 11–22. [[CrossRef](#)]
16. Fragassa, C.; Pavlovic, A.; Santulli, C. Mechanical and impact characterization of flax and basalt fiber vinyl ester composites and their hybrids. *Compos. Part B Eng.* **2018**, *137*, 247–259. [[CrossRef](#)]
17. Lee, J.; Bhattacharyya, D.; Zhang, M.Q.; Yuan, Y.C. Mechanical properties of a self-healing fiber reinforced epoxy composites. *Compos. Part B Eng.* **2015**, *78*, 515–519. [[CrossRef](#)]
18. Dhand, V.; Mittal, G.; Rhee, K.Y.; Park, S.-J.; Hui, D. A short review on basalt fiber reinforced polymer composites. *Compos. Part B Eng.* **2015**, *73*, 166–180. [[CrossRef](#)]
19. Kubiak, T.; Kaczmarek, L. Estimation of load-carrying capacity for thin-walled composite beams. *Compos. Struct.* **2015**, *119*, 749–756. [[CrossRef](#)]
20. Malik, M.H.; Arif, A.F.M.; Al-Sulaiman, F.A.a.; Khan, Z. Impact resistance of composite laminate flat plates—A parametric sensitivity analysis approach. *Compos. Struct.* **2013**, *102*, 138–147. [[CrossRef](#)]
21. Malik, M.; Arif, A. ANN prediction model for composite plates against low velocity impact loads using finite element analysis. *Compos. Struct.* **2013**, *101*, 290–300. [[CrossRef](#)]
22. Artero-Guerrero, J.A.; Pernas-Sánchez, J.; Martín-Montal, J.; Varas, D.; Lopez, J. The influence of laminate stacking sequence on ballistic limit using a combined Experimental/FEM/Artificial Neural Networks (ANN) methodology. *Compos. Struct.* **2018**, *183*, 299–308. [[CrossRef](#)]
23. Riccio, A.; Di Felice, G.; Saputo, S.; Scaramuzzino, F. Stacking Sequence Effects on Damage Onset in Composite Laminate Subjected to Low Velocity Impact. *Procedia Eng.* **2014**, *88*, 222–229. [[CrossRef](#)]
24. Kessler, M.R. *Advanced Topics in Characterization of Composites*; Trafford Publishing (UK) Ltd.: Victoria, BC, Canada, 2004.
25. Cucinotta, F.; Guglielmino, E.; Risitano, G.; Sfravara, F. Assessment of Damage Evolution in Sandwich Composite Material Subjected to Repeated Impacts by Means Optical Measurements. *Procedia Struct. Integr.* **2016**, *2*, 3660–3667. [[CrossRef](#)]
26. Gunasegaran, V.; Prashanth, R.; Narayanan, M. Experimental Investigation and Finite Element Analysis of Filament Wound GRP Pipes for Underground Applications. *Procedia Eng.* **2013**, *64*, 1293–1301. [[CrossRef](#)]
27. Yang, R.; He, Y. Optically and non-optically excited thermography for composites: A review. *Infrared Phys. Technol.* **2016**, *75*, 26–50. [[CrossRef](#)]
28. Rios, A.D.S.; De Amorim Júnior, W.F.; De Moura, E.P.; De Deus, E.P.; Feitosa, J.P.D.A. Effects of accelerated aging on mechanical, thermal and morphological behavior of polyurethane/epoxy/fiberglass composites. *Polym. Test.* **2016**, *50*, 152–163. [[CrossRef](#)]
29. Castellano, A.; Fraddosio, A.; Piccioni, M.D. Ultrasonic goniometric immersion tests for the characterization of fatigue post-LVI damage induced anisotropy superimposed to the constitutive anisotropy of polymer composites. *Compos. Part B Eng.* **2017**, *116*, 122–136. [[CrossRef](#)]
30. De Fenza, A.; Petrone, G.; Pecora, R.; Barile, M. Post-impact damage detection on a winglet structure realized in composite material. *Compos. Struct.* **2017**, *169*, 129–137. [[CrossRef](#)]
31. Farooq, U.; Myler, P. Prediction of load threshold of fiber-reinforced laminated composite panels subjected to low-velocity drop-weight impact using efficient data filtering techniques. *Results Phys.* **2015**, *5*, 206–221. [[CrossRef](#)]
32. Fang, H.; Gutowski, M.; DiSogra, M.; Wang, Q. A numerical and experimental study of woven fabric material under ballistic impacts. *Adv. Eng. Softw.* **2016**, *96*, 14–28. [[CrossRef](#)]
33. Zhikharev, M.V.; Sapozhnikov, S.B. Two-scale modeling of high-velocity fragment GFRP penetration for assessment of ballistic limit. *Int. J. Impact Eng.* **2017**, *101*, 42–48. [[CrossRef](#)]

34. Usta, F.; Mullaoglu, F.; Türkmen, H.S.; Balkan, D.; Mecitoglu, Z.; Kurtaran, H.; Akay, E. Effects of Thickness and Curvature on Impact Behaviour of Composite Panels. *Procedia Eng.* **2016**, *167*, 216–222. [[CrossRef](#)]
35. Jang, B.; Kowbel, W.; Jang, B. Impact behavior and impact-fatigue testing of polymer composites. *Compos. Sci. Technol.* **1992**, *44*, 107–118. [[CrossRef](#)]
36. Abrate, S. *Impact engineering of composite structures*; Springer: Berlin, Germany, 2011.
37. ANSYS. *ANSYS LS-DYNA User's Guide, Release 12.1*; ANSYS Inc.: Canonsburg, PA, USA, 2009.
38. Card, M.F.; Wall, L.D., Jr. *NASA-TN-D-6140, L-7058: Torsional Shear Strength of Filament-Wound Glass-Epoxy Tubes*; National Aeronautics and Space Administration: Washington, DC, USA, 1971.



© 2020 by the authors. Licensee MDPI, Basel, Switzerland. This article is an open access article distributed under the terms and conditions of the Creative Commons Attribution (CC BY) license (<http://creativecommons.org/licenses/by/4.0/>).